The 0.7 structure in cleaved edge overgrowth wires

2008 J. Phys.: Condens. Matter 20 164204

(http://iopscience.iop.org/0953-8984/20/16/164204)

J. Phys.: Condens. Matter **20** (2008) 164204 (9pp) doi:10.1088/0953-8984/20/16/164204

The 0.7 structure in cleaved edge overgrowth wires

R de Picciotto[1], K W Baldwin, L N Pfieffer and K W West

Bell Laboratories, Alcatel-Lucent Incorporated, Murray Hill, NJ, USA

E-mail: rafi.depicciotto@gmail.com

Received 1 October 2007, in final form 31 October 2007
Published 1 April 2008
Online at stacks.iop.org/JPhysCM/20/164204

Abstract

We study the conductance through long and ultra-clean one-dimensional conductors and find a conductance anomaly at low charge densities—similar to the so-called 0.7 structure found in short constrictions. Our wires, afforded by the cleaved edge overgrowth technique, allow a quantitative study of this phenomenon in long wires. We find that this anomaly occurs whenever the kinetic energy provided to the carriers exceeds the Fermi energy. In this regime, the measured conductance is found to exceed the value naively expected from non-interacting models.

(Some figures in this article are in colour only in the electronic version)

1. Introduction

The 0.7 structure is a conductance anomaly observed in ballistic one-dimensional constrictions [1] and wires [2]. In such semiconductor devices, one dimensionality is achieved by confinement of charge in the two spatial directions perpendicular to the direction of current flow—leading to a set of quasi-one dimensional subbands separated by energy gaps. The conductance in such systems has been studied extensively both experimentally and theoretically over the years. The hallmark of the behaviors found is the quantization of the linear conductance [3], which equals the conductance quantum $g_0 = 2e^2/h$ multiplied by the number of available transverse modes (spin degeneracy is included explicitly in g_0). In a real device, the occupation of these transverse modes is achieved by controlling the charge density. Successive modes are populated as the Fermi energy is increased to surmount the subband energy gaps at low temperatures. Thus, a plot of the conductance versus density exhibits a series of conductance steps. The 0.7 structure is a deviation from this regular behavior [1, 2, 4]. At elevated temperatures, a weak additional conductance step is observed at low electron densities. The value of the conductance in this density range equals roughly 70% of the quantized plateau value—hence the name of the phenomenon. The same conductance glitch is also observed in the differential conductance in the presence of a large source–drain bias. Here, however, in addition to a differential conductance step at $\sim 0.7 g_0$, yet another flat appears at even lower densities with a differential conductance of some 25–50% of g_0.

We have studied this phenomenon in long wires afforded by a unique crystal growth technique detailed below. The geometry of our wires, with a length to diameter ratio in the 200–600 range, is more amenable to analysis in terms of a uniform one-dimensional charge density inside the device. This advantage has facilitated a quantitative analysis of the observed behaviors, the conclusions of which can be summarized as follows:

(a) The 0.7 structure is a property of long wires. Long both from the geometrical perspective (large aspect ratio) and also in the sense that there are numerous (up to $\sim$100) electrons in the wire under the conditions that the 0.7 structure is observed. Its main characteristics appear to be dependent on charge *density* in the wire and not its length.
(b) The 0.7 structure occurs at densities low enough such that the Fermi energy is much smaller than temperature. The parameter, T/T_F (with T_F the Fermi temperature) is found to exceed $\sim 2\frac{1}{2}$ in this regime—far from being a small parameter.
(c) When induced by increasing the source–drain bias at low temperatures, the 0.7 structure commences when the bias greatly overwhelms the Fermi energy.
(d) Both in the low-temperature high-bias case and in the high-temperature linear-response case, the measured differential conductance is *larger* than the value expected from non-interacting electrons of this density when propagating through a perfect (reflection free) wire.

[1] Address for correspondence.

These findings stipulate contrasting the data with models that account for these unusual circumstances: either very far from equilibrium or at high temperatures—comparable or exceeding the Fermi energy. Clearly, models that ignore correlations are insufficient, as their predictions underestimate the observed conductance. Other models brought forth in recent years [5] are to a large extent unsuited for the extreme conditions we find to be relevant—because they are tailored either for short constrictions or for lower temperatures than the range studied here. On the other hand, analysis of the behavior of a one-dimensional electron liquid in these regimes is difficult and available knowledge is limited.

Even with wires in the limit of zero temperature difficulties arise due to the inadequacy of Fermi liquid theory [6] in one dimension; the decay rate of Fermi liquid quasi-particles as estimated by the Fermi golden rule vanishes—invalidating such an approach. This difficulty can be overcome by adopting a linear approximation for the dispersion relation. Then the problem can be solved exactly to result in the celebrated Tomonaga–Luttinger model [7]. The resulting unusual liquid possesses no single particle excitations, replaced by collective ones in the form of charge and spin density waves. However, a linear dispersion approximation is inadequate with temperature or bias exceeding the Fermi energy, where the 0.7 structure is observed. A recent work [8] has shown that accounting for a dispersion curvature perturbatively (in T/T_F) already leads to surprising consequences as Fermi liquid like features reappear in the spectral function, coexisting with Luttinger liquid signatures.

Another difficulty with the parameters range of interest here is our poor understanding of relaxation mechanisms and the resultant steady state distribution function in a long wire. In the absence of any relaxation, the distribution function inside a ballistic wire will encompass two separate Fermi distribution functions for left and right propagating electrons, each species being in thermal equilibrium with the reservoir it emanated from. In a diffusive metal, two-particle e–e scattering is an effective channel to relax such a distribution function [9], ultimately resulting in a Fermi function of an elevated (position dependent) electronic temperature. Inelastic processes involving phonons further relax the distribution function, bringing the electron temperature closer to the lattice one. With one-dimensional wires, however, it is well known that because of momentum and energy conservation two body e–e collisions cannot relax the distribution function, as they merely amount to swapping the two electrons. Still, an elevated temperature could facilitate three body collisions that do not suffer from this shortcoming and may modify the distribution function. The leading correction (again in T/T_F) to the conductance due to such three particle collisions was recently calculated in [10]. The authors find conductance suppression to values below the non-interacting one—opposite to the observed 0.7 structure. The discrepancy is not surprising, as the small parameter used in the calculation is not at all small in the experiments—being larger than 2.5 in the density range where the 0.7 structure is observed.

Evaluating the steady state distribution function in a long one-dimensional wire and predicting its transport properties far from the low-temperature linear-response limit while accounting for a realistic parabolic dispersion relation remains challenging. The observed phenomena are richer than naively expected with the 0.7 structure discussed here representing one example of a phenomenon occurring in reduced dimensional mesoscopic structures under such circumstances.

The reminder of this manuscript is arranged as follows; in section 2 we describe the devices used, their fabrication technique and some of their low temperature and linear response characteristics. In section 3 we describe the 0.7 structure as observed in the non-linear response of our wires at low temperatures. Section 4 describes the results obtained in linear response at elevated temperatures and section 5 details the dependence of these latter results on a magnetic field. We summarize the results in section 6.

2. Cleaved edge overgrowth wires

Cleaved edge overgrowth [11] (CEO) is a technique that enables the fabrication of long, uniform and ultra-clean one-dimensional wires for research. The wires formed are characterized by tight confinement and a large subband separation. The channel transverse dimension can be made as narrow as ∼100 Å and the separation between the 1st and 2nd subbands can be as large as ∼150 K [2]. In addition, the wires are ultra-clean, with ballistic transport observed in wires as long as 20 μm [12]. A gate electrode stretched uniformly some 1/2 μm away from the channel controls the charge density in the wire. With this geometry the charge density in the wire, n, is expected to be uniform, given by $n = \frac{c}{e}(V_g - V_{th})$ where c is the gate-channel capacitance per unit length, V_g is the gate voltage and the threshold gate voltage, V_{th}, is the gate voltage required to deplete the wire at low temperatures. As we will show below, this specific capacitance in our devices is rather small, necessitating large gate voltages in the density range of interest. Therefore, corrections to this capacitance, stemming from the finite compressibility and its temperature dependence [13], are negligible. This simple relation between the gate voltage and the density, also verified via direct experimentation in CEO wires [15], is a central and recurring theme in this manuscript. A measurement of the specific capacitance allows us to infer the charge density and hence the Fermi energy at all gate voltages and facilitates direct quantitative comparison to theoretical models.

The wires are fabricated from a GaAs/AlGaAs heterostructures as illustrated in figure 1. The fabrication starts with a high quality 2DEG created by molecular beam epitaxy (MBE) growth of a unilaterally doped GaAs quantum well (QW) onto a [001] GaAs substrate. The resultant 2DEG has a carrier density $n_s \approx 2.5 \times 10^{11}$ cm^{-2}, and mobility $\mu \approx 4 \times 10^6$ cm^2 V^{-1} s^{-1}. Subsequently, this wafer is cleaved inside the MBE chamber to expose a clean and atomically smooth [110] surface, which is immediately overgrown with a modulation-doped epitaxial layer sequence. The additional remote Si dopants that are introduced by this overgrowth step lead to a higher electron density near the cleaved edge of the QW. As in conventional modulation-doped samples, a strong built in electric field binds this excess charge to the cleaved

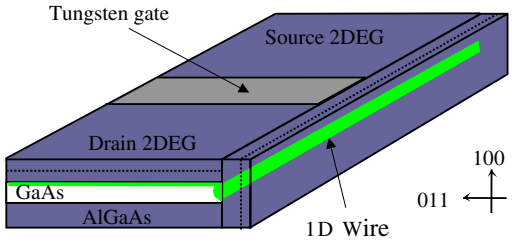

Figure 1. Geometry of the CEO device: a high quality 2DEG is created by MBE growth of a unilaterally doped GaAs quantum well (QW) onto a [001] GaAs substrate. This wafer is then cleaved inside the MBE chamber and a 2nd modulation-doped epitaxial layer sequence is immediately overgrown onto the freshly exposed [110] surface. The Si dopants that are introduced by this overgrowth step lead to a higher electron density along one edge of the 2DEG. As in conventional modulation-doped samples, a strong built in electric field binds this excess charge to the cleaved edge interface, creating 1D bound states all along the edge of the GaAs QW. This wire contains ∼10 electronic modes and coexists with a 2DEG that resides in the QW plane and couples to the wire from the side. To separate the 2DEG from the wire, pre-fabricated tungsten gate electrodes are used to deplete the 2DEG underneath but preserve the 1D channel in this region along the edge. The width of the tungsten gate thus defines the length of the isolated wire section (see text).

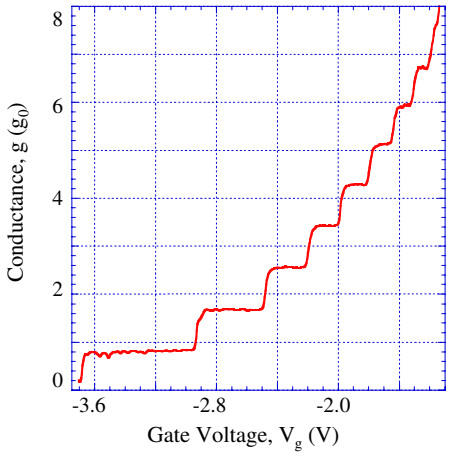

Figure 2. A representative result of a 2-terminal conductance measurement of a CEO wire at a temperature, $T \approx 300$ mK. A voltage applied to a nearby gate forms a 2 μm long wire and controls its charge density (see figure 1). Clear conductance plateaus arise, attesting to the high quality of the wire. The value of the quantized resistance is somewhat larger than the universal value of R_0 [12]. The origin of this deviation is non-ideal coupling between the CEO wire and its 2DEG source and drain contacts [14] (see text).

edge interface, creating 1D bound states all along the edge of the GaAs QW. This wire contains ∼10 electronic modes and coexists with a 2DEG that resides in the QW plane and couples to the wire from the side.

A pre-fabricated top gate electrode (see figure 1) allows shaping of the 2DEG sheet. Biasing the gate depletes the 2DEG underneath and creates a stretch of one-dimensional wire in front of it, which is now separated from the 2DEG. The width of the gate defines the length of this isolated wire section while the 2DEG areas on either side conveniently serve as source and drain contacts to the wire. This geometry lends itself to a straightforward two-probe measurement on a quantum wire. Figure 2 shows the high quality, quantized conductance steps observed in such a specimen as successive 1D subbands are being depopulated.

The conductance values at these plateaus, however, are smaller than expected (g_0 multiplied by the number of modes, see figure 2). This trend has been repeatedly observed in numerous CEO wires of various lengths (not shown). It has been established via direct measurements [12] that this conductance deficiency (excess resistance) does not come about due to backscattering inside the wire. In fact a four terminal resistance measurements with such wires have revealed no significant resistance internal to the wire [14]. The excess resistance rather reflects an imperfect coupling between the wire and the reservoirs—falling slightly short of perfect adiabatic coupling. This contact resistance is potentially both temperature and bias dependent, a fact that complicates quantitative assessments pertaining to the 0.7 structure that will be addressed in the following sections. To circumvent such difficulties, we concentrate mostly on the dependence of the phenomenon observed on the charge density in the wire—a study that has proven to be instructive in its own right.

3. Non linear response of cleaved edge overgrowth wires

The trace of the linear conductance shown in figure 2 exhibits a series of regular quantized conductance plateaus. This quantization of the linear conductance in ballistic wires is a robust phenomenon—insensitive to the system details. All that is required is the absence of backward scattering inside the wire and adiabatic feeding of charge from the reservoirs into the wire. This regular picture, however, becomes more complex when the differential conductance is measured in the presence of a large source–drain bias [1, 2] as shown in figure 3(a).

At low bias, the linear conductance exhibits weak modulations with gate voltage about its mean value of $\sim 0.85 g_0$. As the bias is increased, the mean differential conductance increases while the oscillatory structure diminishes. Instead, a conductance peculiarity emerges at low densities. Similar to the 0.7 structure data observed in split gate constrictions, this feature becomes more pronounced at larger applied biases. As can be seen in figure 3(a), the conductance is a non-monotonic function of the gate voltage in this range, with a mean value of about 70% of its plateau value[2]. This conductance feature is distinct from yet another conductance step, which occurs at a conductance of $\sim 0.25 g_0$ in our wires (see figure 3(a)).

We proceed by calculating the numerical derivative of the differential conductance with respect to the gate voltage (at fixed bias)—as shown in figure 3(b). This serves two purposes: first, this quantity measures the sensitivity of the conductance to the charge density *in the wire*. Therefore, the bias dependence of the contact resistance, which is associated

[2] The non-monotonic conductance behavior diminishes at elevated temperature. Above $T \sim 2$ K we observe the more common 0.7 conductance step (data not shown).

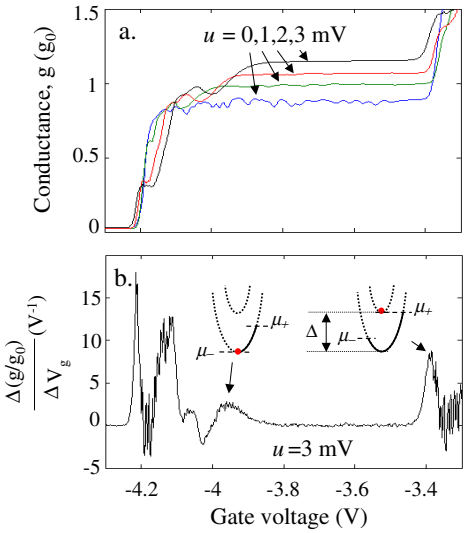

Figure 3. Differential conductance versus gate voltage at different biases. (a) Differential conductance of a 2 μm long CEO wire at a bath temperature of 18 mK. An AC excitation of 18 μV was used in conjunction with a DC bias of 0, 1, 2, 3 mV—blue, green, red and black lines, respectively. The conductance anomaly at low densities is more pronounced at a larger source–drain bias. (b) The numerical derivative of the differential conductance at a 3 mV bias (black trace in (a)), with respect to the gate voltage. This quantity highlights the transitions between different conductance values, as shown. Inset: the conductance plateau is bound by the 2nd subband at high densities and by depletion of left movers at low densities—see text.

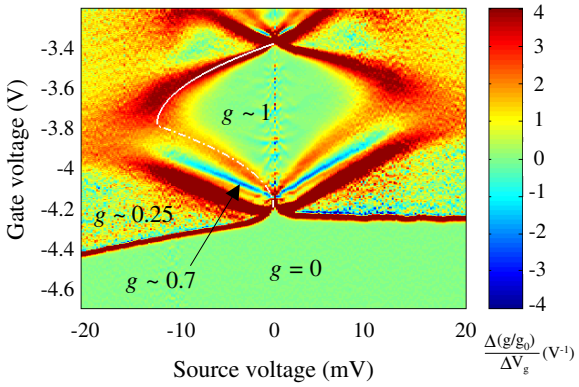

Figure 4. Trans-conductance versus gate voltage and DC bias: the numerical derivative of the differential conductance with respect to gate voltage (see figure 3(b)) as a function of gate voltage and DC bias, in a color plot format. Data where taken with an AC excitation of 18 μV at a bath temperature of 18 mK. The red streaks separate regions of different conductance values, as indicated. The data is largely symmetric with respect to the applied bias. The slight asymmetry results from unintentional device asymmetry that varied from device to device (not shown). Superimposed on the data are the curves $u_\Delta(V_g)$—solid white line, and $u_0(V_g)$—dashed dotted white line (see text). The onset of the 0.7 anomaly corresponds to the $u_0(V_g)$ curve, which marks the depletion of left (right) movers at a positive (negative) bias (see figure 3(b) inset).

with the non-gated regions where the 1D density is fixed, is eliminated form the resultant data. Second, this derivative highlights the gate voltages where transitions between different conductance values occur. It therefore allows us to follow the conductance changes with both gate voltage and bias—as shown in a color-plot format in figure 4. The color-coding is such that red streaks in the data correspond to large derivative and thus separate regions of different conductance values, as indicated. Within each region the gate voltage dependence of the differential conductance is weak.

The lowest red streak in figure 4 separates the zero-conductance state, with a depleted wire, from the finite conductance regions. This pinch off line exhibits a cusp at small biases. In addition, the aforementioned weak conductance oscillations are visible in the same bias range, at larger gate voltages. Both phenomena disappear at an elevated temperature of 4.2 K (not shown). These features are inconsequential for the analysis in the following sections and will therefore be ignored.

We now turn to a simple model for transport in a ballistic wire in order to analyze the observed behaviors. The relevance of this simple-minded model stems from the data, as will be shown below. We consider free electrons induced by a nearby gate into a clean 1D channel, which is coupled adiabatically to two reservoirs. The Fermi energy in the wire is $\varepsilon_F = \hbar^2 k_F^2/2m$, where m is the effective mass of an electron and the Fermi wavevector, k_F, is related to the electron density and hence to the gate voltage via: $k_F = \frac{\pi}{2} n = \frac{\pi}{2}\frac{c}{e}(V_g - V_{th})$. A finite energy gap, Δ, separates the lowest wire mode from the 2nd subband.

In order to facilitate an electrical current, an imbalance between the electrochemical potentials of the source (right) and drain (left) reservoirs is imposed. This bias, in turn, establishes a difference between the chemical potentials of the left and right propagating electrons in the wire (μ_+ and μ_- respectively): $\mu_+ - \mu_- = eu$, with u the applied bias. Importantly, the charge density in the wire is nearly independent of this bias—remaining almost equal to the equilibrium one. This arises because with a small gate-wire capacitance, a large potential energy penalty is associated with charge imbalance. Charge neutrality is thus facilitated by a uniform shift of the potential in the wire, such that $n_+ + n_- = n$ or $\sqrt{\mu_+} + \sqrt{\mu_-} = 2\sqrt{\varepsilon_F}$. This potential shift reflects the *screening* of the applied bias by the free charges and is accomplished by two potential steps at the inlet and at the outlet of the wire. Note that this potential shift equals half the applied voltage [14] only at voltages much smaller than the Fermi energy where particle–hole symmetry prevails.

At moderately low biases, the considerations above are sufficient to calculate the two chemical potentials: $\mu_\pm = \varepsilon_F(1 \pm \frac{eu}{4\varepsilon_F})^2$. These potentials are both bias and density dependent, with the density dependence encoded in ε_F. Thus, as the bias is increased two distinct situations may occur, depending on density:

(a) For $\varepsilon_F \geqslant \frac{1}{4}\Delta$, a bias $u_\Delta = \frac{4\varepsilon_F}{e}(\sqrt{\Delta/\varepsilon_F} - 1)$ will enforce $\mu_+ = \Delta$. Thus, a bias $u > u_\Delta$ allows the 2nd subband to participate in transport and an increased conductance is expected (see figure 3(b)).

(b) Alternatively, for $\varepsilon_F \leqslant \frac{1}{4}\Delta$, a bias as large as $u_0 = 4\varepsilon_F/e$ will impose $\mu_- = 0$. With such a bias, the electrons in the wire are unidirectional and the entire

population propagates in the same direction—accounting for the current (see figure 3(b)).

Indeed, we find that the line marking an increase in the differential conductance beyond its plateau value corresponds well to the curve $u_\Delta(V_g)$—as shown by the solid white line in figure 4. The only free parameter here is the specific capacitance, which we determine to be: $c = 18.5 \pm 0.5$ aF μm^{-1}. This measured value agrees very well with independent measurements via tunneling spectroscopy in very similar structures [15], as well as with estimates based on the known geometry.

Remarkably, we find that at lower densities the curve $u_0(V_g)$, i.e. the bias required for unidirectional dynamics, agrees very well with the high density onset of the 0.7 structure—as shown in the same figure. Thus, the depletion of left (or right) movers marks the occurrence of the 0.7 structure. We emphasize that this curve is simply plotted onto the data in figure 4 (dash–dotted white line) with no additional fitting parameters.

The deduced capacitance amounts to some 115 electrons per micrometer for each 1 V applied to the gate beyond the pinch off value. Therefore, the 0.7 structure features presented in figure 2 span a density of up to $\sim$50 μm^{-1}, or a total of $\sim$100 electrons in our 2 μm long wire. In addition, as we will show in the following section, the 0.7 structure is observed in linear response in our wires at elevated temperatures in excess of 10 K and at such temperatures extends up to densities of $\sim$30 μm^{-1}, again corresponding to a large number of electrons in the wire. Therefore this phenomenon occurs in long one-dimensional wires. Long not only from the geometrical aspect ratio perspective but also in the sense that there are numerous electrons in the wire. We will further show in the next section that the phenomenon appears in exactly the same density range when a 6 μm long wire is used, clearly showing that it represents a property of long one-dimensional wires.

Before turning to the behaviors observed at elevated temperatures we return to the low-temperature non-linear response data discussed above and examine the behavior at even larger electron densities, when more than on subband is occupied. We have taken similar data at larger gate voltages, where the 2nd–6th wire modes are occupied, as shown in figure 5. Evidently these data can be fitted to the same model above, again with a striking level of agreement (see figure 5). However, we find from our fits that the capacitance between the gate to each channel increases by $\sim$10% per channel. This behavior is to be expected because the transverse charge distribution in the wire is controlled by the mode wavefunctions and thus varies with mode index. This 'wire diameter' variation is expected to affect the geometrical part of the capacitance logarithmically. In addition, all the wire modes are coupled, both via a direct capacitive coupling and also because all modes share common reservoirs, dictating a common electrochemical potential.

Drawing an analogy to the capacitance of a coaxial cable, we estimate the capacitance between the gate and the jth mode in our CEO wires as: $c_j = \alpha 2\pi\varepsilon_0\varepsilon_r / \ln(d/\delta_j)$, where δ_j is the half width of the wavefunction of the jth mode, d is

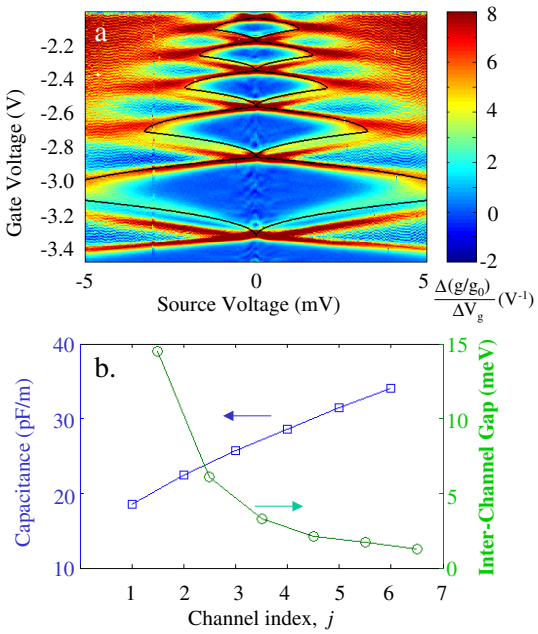

Figure 5. Trans-conductance of the upper wire modes: (a) the numerical derivative of the differential conductance with respect to gate voltage as a function of gate voltage and DC bias in a color plot format. Data where taken with an AC excitation of 18 μV at a bath temperature of 18 mK. The gate voltage range shown corresponds to the 2nd–6th wire modes. Solid lines: $u_\Delta(V_g)$ and $u_0(V_g)$ curves for each one of the wire modes (see text). (b) Left panel, blue squares: the capacitance between the gate and the jth wire mode, as calculated in a simple model (see text), plotted against the mode index. These capacitance values lead to the excellent agreement with the data in figure 3(a) as well as in figure 2. Right panel, green circles: the inter-channel gaps $\Delta_{i\to i+1}$, as deduced from the data. The confinement energy of the 1st mode is $\sim$15 meV.

the distance to the gate and α is a proportionality factor—accounting for the fact that the gate is planar rather than concentric with the wire. Approximating the half width of the jth mode by $\delta_j = j \cdot 100$ Å [14] and using the known wire-gate distance: $d \cong 5000$ Å, we obtain an excellent fit for all the data in both figures 4 and 5(a) with a single fitting parameter: $\alpha = 0.1$. This agreement shows that the overall capacitance is dominated by geometry and the corrections due to the density of states or the inter-mode coupling are negligible, as expected.

Our analysis matches the onset of the 0.7 structure with depletion of either left or right movers in the wire. The conductance value itself ($g \sim 0.7g_0$) remains unexplained. Nor is the existence of yet another flat conductance region ($g \sim 0.25g_0$) clarified. Both features in the differential conductance were observed first in quantum point contact constrictions, where the 2nd flat occurring near $g \sim 0.5g_0$. This latter behavior was explained in [16] by employing a model that assumes a large number, j, of quasi-1D modes present, and thus ignores screening to predict: $g = (j - \frac{1}{2})g_0$, at a bias large enough to establish unidirectional dynamics in the jth mode. Thus, with a single mode and screening ignored, a conductance of $\frac{1}{2}g_0$ is expected in this non-interacting electron model. In contrast, a strictly charge-neutral wire is expected to exhibit a zero differential conductance in this bias range; once the left

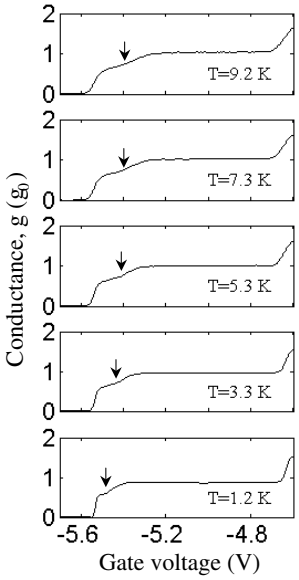

Figure 6. Conductance versus gate voltage at different temperatures: the linear conductance of a 2 μm long CEO wire, measured with an excitation of 30 μV at various temperatures, is plotted against the gate voltage. The conductance, divided here by the quantum conductance, dwells at a value of ∼0.7 over a finite gate-voltage range. This conductance anomaly extends over a wider density range at higher temperatures (arrows).

movers are depleted, the number of right movers is dictated by charge neutrality and since the resultant current, $I_{\max} = 8\frac{e}{h}\mu$, is independent of bias, the differential conductance is expected to vanish. With a finite wire-gate capacitance, a self-consistent solution is likely to yield an intermediate differential conductance; $0 < g < \frac{1}{2}g_0$ and may explain the $g \sim 0.25g_0$ plateau observed here. We emphasize, however, that this plateau occurs at a lower density (or a larger bias) than predicted, while a larger differential conductance value, $g \sim 0.7g_0$, persists over an intermediate parameters range. We may therefore conclude that the 0.7 structure represents an enhanced differential conductance—not accounted for in a non-interacting electron model.

This unique situation of unidirectional electron occupation discussed here is unlikely to occur in linear response at elevated temperatures, where the 0.7 structure is also observed [1, 2]. Yet, this elevated temperature 0.7 structure does share some of the basic characteristics and principles detailed above as will be discussed in the next section.

4. Linear response at elevated temperatures

The temperature dependence of the linear conductance with a 2 μm long wire is shown in figure 6. The 0.7 structure is clearly seen in the data. Similar to QPCs data, this feature becomes more pronounced at higher temperatures, with its density range increasing with temperature. A close inspection of the traces in figure 6 shows that the value of the conductance at the first plateau, g_p, is by itself temperature dependent. It increases from $0.85g_0$ at $T \sim 0.3$ K and saturates to $g_p \approx g_0$ by $T \sim 10$ K for this wire (not shown). This behavior, unique to CEO

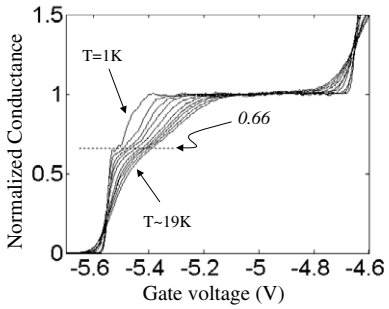

Figure 7. Normalized conductance versus gate voltage at different temperatures: the conductance, normalized to its value at the 1st plateau—g_p, is plotted against the gate voltage. The temperature ranges from 1 to 19 K with 2 K increments between traces. The anomaly occurs at a conductance of 66–68% of the plateau value, regardless of temperature.

wires, results from the temperature dependence of the contact resistance. In the following we will focus on the density and temperature dependence of the 0.7 feature. To circumvent the temperature dependent contact resistance, we may employ the same strategy as in the previous section—differentiating with respect to gate voltage. It turns out, however, that it is sufficient to normalize the conductance gate voltage traces to their plateau values, as shown in figure 7. As can be seen in this figure, the conductance peculiarity always occurs at a conductance value of $\sim 0.66g_p$ regardless of the exact value of the plateau conductance. Clearly, the value of the contact resistance itself is inconsequential. Further, we have been able to observe the same behavior with an even longer (6 μm long) wire and observe practically identical dependence of the conductance on the *density* in the wire as shown in the inset of figure 8. The phenomenon is robust and, to a large extent, independent of the wire length.

We follow the evolution of the 0.7 feature with temperature by measuring the gate voltage, V^*, that marks the transition between the main plateau and the 0.7 structure (see figure 8). We define V^* as the gate voltage where the conductance equals 85% of its plateau value, half way between 0.7 and 1, and follow its temperature dependence. It is worthwhile to evaluate the Fermi energy at this gate voltage, ε_F^*, and discuss the temperature dependence of this Fermi energy. In order to determine the specific capacitance needed to evaluate ε_F^*, we repeated the non-linear transport measurements described in the previous section—with this particular wire and obtained a value of $c = 19 \pm 0.5$ aF μm^{-1}, practically identical to the one reported in the previous section.

In figure 9 we plot ε_F^*, deduced from the measured gate voltages V^*, against temperature for the two different wires measured. As can be seen in this figure, this quantity is simply proportional to temperature. Moreover, the coefficient of proportionality equals unity, namely $\varepsilon_F^* = k_B T$, as illustrated by the solid line in the same figure . Thus, the crossover from the conductance plateau into the 0.7 structure occurs as the carriers in the wire are diluted to form a non-degenerate system.

In order to pinpoint the 0.7 structure parameters regime, we measure another characteristic gate voltage, $\tilde{V}$, which

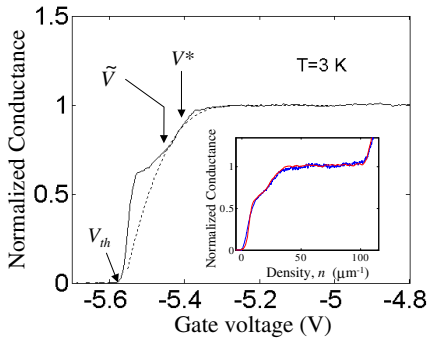

Figure 8. Characteristics of the 0.7 structure: the conductance at $T = 3$ K, normalized to its plateau value, is plotted against the gate voltage. Two characteristic gate voltages are indicated (arrows): V^* corresponds to the transition between the plateau and the 0.7 structure, and $\tilde{V}$ marks the high-density extent of this feature (see text). The threshold gate voltage, $V_{\rm th}$ is also indicated. These quantities are use in conjunction with the specific capacitance to deduce the charge density in the wire. The expected conductance within a free electron model is easily calculated once the density is known (see text). The resulting curve (dotted line) is added onto the data and is seen to underestimate the measured conductance at low densities. Inset: comparison between wires of different length: we portray the conductance of a 2 μm long wire (red solid line (in the electronic version of the journal)) and that of a 6 μm long one (blue solid line (in the electronic version of the journal)), both plotted against the density in the wire. The behavior is identical to within our ability to determine zero density. Data were taken at a temperature of 6.74 and 7.00 K, respectively. The density was deduced from the deviation of the gate voltages from the pinch off values (different for the two wires) and using the same specific capacitance (18.5 aF μm^{-1}). The conductance was normalized to its respective plateau value ($0.7g_0$ and g_0 for the 6 and 2 μm long wire, respectively).

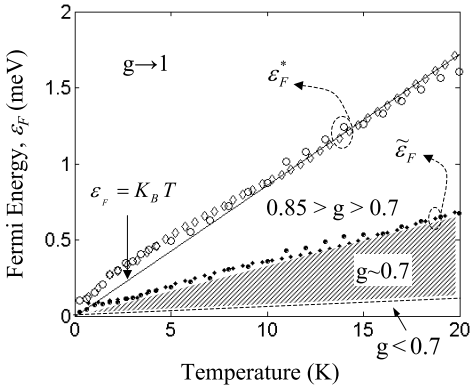

Figure 9. Phase diagram of the 0.7 structure: the Fermi energy in the wire at the transition between the plateau and the 0.7 structure—$\varepsilon_{\rm F}^* = \varepsilon_{\rm F}(V_{\rm gate} = V^*)$ (open symbols) and the one marking the high density edge of this feature—$\tilde{\varepsilon}_{\rm F} = \varepsilon_{\rm F}(V_{\rm gate} = \tilde{V})$ (filled symbols) are plotted against temperature. Data were taken from two different wires, both 2 μm long (diamonds and circles). The data appear linear in this energy–temperature plane, attesting to the 1D nature of our device. The line $\varepsilon_{\rm F} = k_{\rm B}\,T$ is added onto the data (solid line) and is seen to match $\varepsilon_{\rm F}^*$. The shaded area at the bottom of the figure corresponds to the 0.7 structure region—clearly in the non-degenerate regime. The measured conductance dwells at $g \sim 0.7$ down to very low 1D densities (see footnote 3), as illustrated by the dashed line.

corresponds to the extent of the 0.7 structure itself (see figure 8). Since the 0.7 structure in our wires occurs when the conductance equals 66–68% of the plateau value, we defined $\tilde{V}$ as the gate voltage where the normalized conductance equals 0.69. In other words, $\tilde{V}$ is defined such that the conductance anomaly occurs in the density range $0 \approx n \leqslant n(V_{\rm g} = \tilde{V})$.[3] We plot the corresponding Fermi energy against temperature in the same figure. Clearly, the 0.7 structure occurs deep in the non-degenerate regime; $k_{\rm B}T \geqslant 2\frac{1}{2}\varepsilon_{\rm F}$. It is interesting to note that the 0.7 structure occurs when the occupation of zero momentum states, at the bottom of the subband, is not saturated. This is true whether this arises due to a high enough temperature or a large enough bias—as in the previous section. Clearly the curvature of the dispersion relation is important in both cases.

We now turn to a comparison between the data and the conductance expected in a non-interacting model. Surely the conductance through a wire vanishes when it is depleted of charge, regardless of correlations. It is the way that the measured conductance diminishes with density at a finite temperature that we would like to compare to a non-interacting model. With free electrons in a reflection free single mode wire, the well-known cancelation between the velocity and the density of states leads to a simple expression for the linear conductance: $g/g_0 = f(\varepsilon = 0)$, where $f(0) = 1/(1 + {\rm e}^{\frac{-\mu}{k_{\rm B}T}})$ is the Fermi function evaluated at zero energy: the chemical potential is related to temperature and density via: $n = \int_0^\infty {\rm d}\varepsilon\,[\nu(\varepsilon) f((\varepsilon - \mu)/k_{\rm B}T)]$ where $\nu(\varepsilon) = 2/h\sqrt{2m/\varepsilon}$ is the density of states.

We have evaluated this chemical potential numerically and added the resultant conductance trace onto the data in figure 8. Evidently, the fact that the conductance decreases significantly below its plateau value as the Fermi energy is reduced by the gate voltage to match $k_{\rm B}T$ is not very surprising and is in fact expected from this model. The surprising feature is the *excess of conductance* at lower densities. Similar to the low-temperatures non-linear response described in the previous section, here again the measured conductance is *too high* to be accounted for by a free-electron model.

5. Magnetic field dependence

The magnetic field dependence of the linear conductance was measured with a magnetic field, B, aligned (to within $\sim 3°$) along the current flow direction in a 2 μm long wire. Traces of the conductance versus gate voltage at a few selected magnetic fields and a temperature $T \sim 250$ mK are portrayed in figure 10. With increasing field, the 0.7 structure evolves into a wider conductance step with its value decreasing with field to equal $\frac{1}{2}g_0 = e^2/h$ in the high field limit [17].

This high field behavior is to be expected; a magnetic field lifts the spin degeneracy and splits each subband into two spin branches separated by a Zeeman gap $\Delta_{\rm spin} = g\mu_{\rm B}B$. Here $\mu_{\rm B}$ is the Bohr magnetron and g is the electronic

[3] The conductance declines toward zero when the density in the wire is very small, 2–3 times smaller than the one at the high-density edge of the 0.7 structure. Therefore, this feature extends to a Fermi energy as small as $\sim k_{\rm B}T/15$.

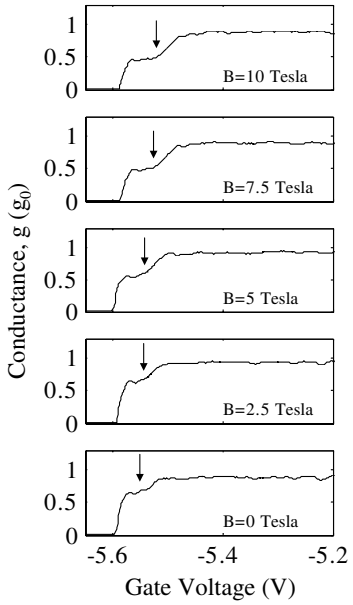

Figure 10. Conductance versus gate voltage at different magnetic fields: the linear conductance of a 2 μm long CEO wire, measured in the presence of a magnetic field (as indicated), is plotted against the gate voltage. The magnetic field was aligned along the wire. The 0.7 conductance anomaly evolves into a $1/2$ plateau that extends over a wider density range as indicated by arrows (see text).

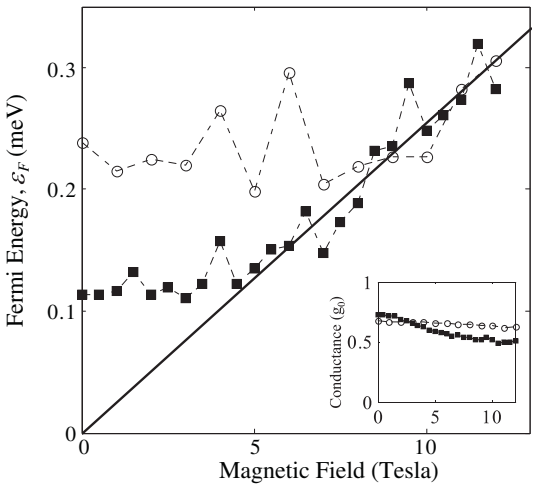

Figure 11. Evolution of the 0.7 structure with magnetic field: the Fermi energy at the onset of conductance increase beyond its step value is plotted against magnetic field. This Fermi energy was calculated from the gate voltages, $\hat{V}_{\rm gate}$, (see figure 9) extracted from data taken at $T \sim 250$ mK (solid squares) and 1.5 K (open circles). Complete spin polarization is assumed for the purpose of evaluating $\hat{\varepsilon}_{\rm F}$. The line $\hat{\varepsilon}_{\rm F} = g\mu_{\rm B}B$ is added onto the data (solid line) and agrees very well with the $T \sim 250$ mK data beyond a field of ~5 T (see text). Inset: the value of the conductance step is plotted against field. Data was taken at $T \sim 250$ mK (solid squares) and 1.5 K (open circles). The low-temperature conductance value is seen to evolve with field from ~0.7 to 0.5 with the same characteristic field of ~5 T (the values in the inset's abscissa refer to the magnetic field in tesla).

g-factor. Therefore one would expect (within this non-interacting picture) that in the density range where only one (spin resolved) subband is populated the conductance would acquire a half step value—reflecting the reduction in subband degeneracy. This is expected to occur in the density range where the Fermi energy is smaller than the Zeeman gap. Note that the lifting of spin degeneracy also affects the Fermi wavevector—being twice as large as the zero field value. Therefore the spin-polarized Fermi energy is four fold larger; $\varepsilon_{\rm F}^{\rm sp}(n) = 4\varepsilon_{\rm F}(n)$.

We have measured the gate voltages, $\hat{V}_{\rm g}$, corresponding to the onset of conduction increase from its 0.7 structure plateau value. In the absence of a magnetic field this gate voltage matches the high-density extent of the 0.7 structure ($\tilde{V}_{\rm g}$ in the previous section). Therefore in essence we are following the evolution of this gate voltage with field. Employing the known gate-channel capacitance, we have calculated the spin-polarized Fermi energy for each applied magnetic field data set. The evolution of this quantity with magnetic field is depicted in figure 11. This maximal Fermi energy, $\hat{\varepsilon}_{\rm F}^{\rm sp}$, increases with field and acquires a linear field dependence at high fields beyond a characteristic field of $B \approx 5$ T. We find that this linear field dependence matches the expected behavior $\hat{\varepsilon}_{\rm F}^{\rm sp} = g\mu_{\rm B}B$ with $g = -0.44$, the bulk GaAs electronic g-factor (see figure 11). This agreement further corroborates the value of the specific capacitance value, independently deduced from non-linear transport data. The value of the 0.7 structure conductance step also evolves with field. It reduces with field and saturates to a value of $\frac{1}{2}g_0$ at high fields, with the same characteristic field. This behavior is illustrated in the inset of figure 11.

We have repeated this entire procedure at higher temperatures and found that the characteristic magnetic field increases with temperature, quickly escaping our available field window ($B \leqslant 12$ T) at a moderate temperature of ~2 K. The behavior at $T = 1.5$ K was added to figure 11 and its inset to illustrate this behavior. This behavior comes about due to the smallness of the g-factor in GaAs, which in turn has prevented us so far from examining in detail the pinch off characteristics of a spin-polarized wire: an interesting question is whether an analog of the 0.7 structure can be observed in the spin-polarized case. There is no evidence to such $0.7\frac{e^2}{h}$ behavior to date. However, achievable ratios of the Zeeman gap to temperature are much smaller than the ratio of subband gap to temperature in the absence of a magnetic field. We are therefore limited to a smaller parameters window with spin-polarized electrons. One can of course reduce the temperature to allow a larger Zeeman energy to temperature ratio. However this strategy will push the density range where this alleged feature would exist to ever lower densities. With such low densities one would need much longer wires to accommodate even a handful of electrons, a task too difficult currently even with our ultra-clean CEO wires. This question therefore awaits experimentation at larger magnetic fields or cleaner and longer wires.

Finally, we would like to clarify a point that has been confusing for us at first. Within a non-interacting model and in the limit of zero temperature, the Fermi energy at low densities increases with field as spin polarization commences and spin degeneracy is lifted. One could therefore question our conclusions that the 0.7 structure occurs in linear response

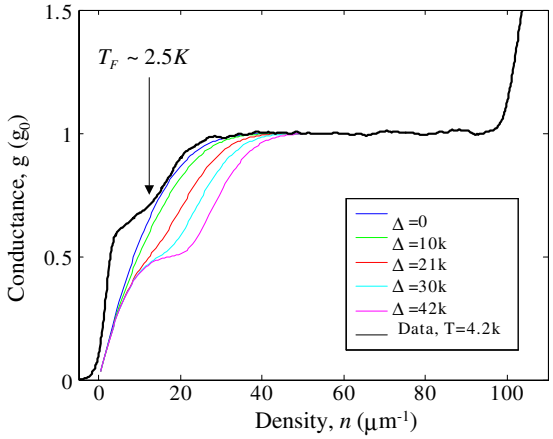

Figure 12. The evolution of the non-interacting conductance with magnetic field at a finite temperature: the conductance in the presence of a spin gap and at a temperature of 4.2 K was calculated within a non-interacting model (see text). The resultant traces (color lines (in the electronic version of the journal) as indicated in legend) are added to a plot of the measured conductance (solid black curve). The applied gate voltage is translated to an electron density via the specific capacitance, independently deduced from non-linear response (see text). This plot clearly shows that the observed conductance is larger than the one expected in a non-interacting model, regardless of spin polarization.

when the Fermi temperature is more than two fold smaller than temperature and that the observed conductance is larger than the expected value. This line of thought, however, is incorrect because spin polarization also causes halving of the conductance due to the same lifting of degeneracy. The net effect is a reduction of the conductance with spin polarization at a given density and temperature. The expected behavior at a temperature of 4.2 K and various spin gaps is illustrated in figure 12, where these results are contrasted with data taken at the same temperature and at zero magnetic field. The curves where calculated along the same lines described in section 4, accounting for two separate spin bands separated by a gap Δ and sharing a single electrochemical potential. Clearly the conductance measured at low density is larger than expected from non-interacting electrons, regardless of spin polarization.

6. Summary

Wires fabricated via the cleaved edge overgrowth technique have allowed us to offer a quantitative account of the 0.7 structure. The geometry used facilitated a reading of the applied gate voltage as a uniform charge density in the wire, which is in turn supported by numerous aspects of data taken in gate-wire devices. This simple insight has led us to some striking conclusions. We have found that the conditions under which this phenomenon is observed are far from the low-temperature linear-response regime, commencing when either the temperature or the bias greatly overwhelm the Fermi energy. Further, we find that the non-interacting conductance, unsophisticatedly calculated within a free electron model, underestimates the measured value. This conductance enhancement, presumably due to e–e interactions, remains in our view poorly understood.

References

[1] Thomas K J, Nicholls J T, Simmons M Y, Pepper M, Mace D R and Ritchie D A 1996 *Phys. Rev. Lett.* **77** 135
Kristensen A, Bruus H, Hansen A E, Jensen J B, Lindelof P E, Marckmann C J, Nygård J, Sørensen C B, Beuscher F, Forchel A and Michel M 2000 *Phys. Rev.* B **62** 10950
Reilly D J, Facer G R, Dzurak A S, Kane B E, Clark R G, Stiles P J, Clark R G, Hamilton A R, O'Brien J L, Lumpkin E, Pfeiffer L N and West K W 2001 *Phys. Rev.* B **63** 121311/1
Cronenwett S M, Lynch H J, Goldhaber-Gordon D, Kouwenhoven L P, Marcus C M, Hirose K, Wingreen N S and Umansky V 2002 *Phys. Rev. Lett.* **88** 226805
[2] de Picciotto R, Pfeiffer L N, Baldwin K W and West K W 2004 *Phys. Rev. Lett.* **92** 036805
de Picciotto R, Pfeiffer L N, Baldwin K W and West K W 2005 *Phys. Rev.* B **72** 033319
[3] Wharam D A, Thornton T J, Newbury R, Pepper M, Ahmed H, Frost J E F, Hasko D G, Peacockt D C, Ritchie D A and Jones G A C 1988 *J. Phys. C: Solid State Phys.* **21** L209
van Wees B J, van Houten H, Beenakker C W J, Williamson J G, Kouwenhoven L P, van der Marel D and Foxon C T 1988 *Phys. Rev. Lett.* **60** 848
[4] See also, Rokhinson L P, Pfeiffer L N and West K W 2006 *Phys. Rev. Lett.* **96** 156602
Chiatti O, Nicholls J T, Proskuryakov Y Y, Lumpkin N, Farrer I and Ritchie D A 2006 *Phys. Rev. Lett.* **97** 056601
Roche P, Ségala J, Glattli D C, Nicholls J T, Pepper M, Graham A C, Thomas K J, Simmons M Y and Ritchie D A 2004 *Phys. Rev. Lett.* **93** 116602
DiCarlo L, Zhang Y, McClure D T, Reilly D J, Marcus C M, Pfeiffer L N and West K W 2006 *Phys. Rev. Lett.* **97** 036810
Chung Y, Jo S, Chang D-I, Lee H-J, Zaffalon M, Umansky V and Heiblum M 2007 *Phys. Rev.* B **76** 035316
[5] See e.g., Matveev K A 2004 *Phys. Rev. Lett.* **92** 10681-1
Rejec T and Meir Y 2006 *Nature* **442** 900 and references therein
[6] Nozières P 1997 *Theory of Interacting Fermi Systems* (Reading, MA: Addison-Wesley)
[7] Tomonaga S 1950 *Prog. Theor. Phys.* **5** 544
Luttinger J M 1963 *J. Math. Phys.* **4** 1154
Mattis D C and Lieb E H 1965 *J. Math. Phys.* **6** 375
[8] Khodas M, Pustilnik M, Kamenev A and Glazman L I 2007 http://arxiv.org/abs/cond-mat/0702505v3
[9] See e.g., Nagaev K E 1995 *Phys. Rev.* B **52** 4740
Pothier H, Guéron S, Birge N O, Esteve D and Devoret M H 1997 *Phys. Rev. Lett.* **79** 3490 and references therein
[10] Lunde A M, Flensberg K and Glazman L I 2007 *Phys. Rev.* B **75** 245418
[11] Pfeiffer L N *et al* 1997 *Microelectron. J.* **28** 817–23
[12] Yacoby A, Stormer H L, Wingreen N S, Pfeiffer L N, Baldwin K W and West K W 1996 *Phys. Rev. Lett.* **77** 4612-5
de Picciotto R, Stormer H L, Yacoby A, Pfeiffer L N, Baldwin K W and West K W 2000 *Phys. Rev. Lett.* **85** 1730-3
[13] Ilani S, Donev L A K, Kindermann M and McEuen P L 2006 *Nat. Phys.* **2** 867
Lu Y, Tu R, Wang X, Nishi Y and Dai H 2007 http://arxiv.org/abs/0707.0171v1
[14] de Picciotto R, Stormer H L, Pfeiffer L N, Baldwin K W and West K W 2001 *Nature* **411** 51
[15] Auslaender O M, Yacoby A, de Picciotto R, Baldwin K W, Pfeiffer L N and West K W 2002 *Science* **295** 825
[16] Glazman L I and Khaetskii A V 1988 *JETP Lett.* **48** 591
[17] See also Koop E J, Lerescu A I, Liu J, van Wees B J, Reuter D, Wieck A D and van der Wal C H 2007 http://arxiv.org/abs/0706.0792v1 and references therein